46th AIAA Aerospace Sciences Meeting and Exhibit
7 - 10 January 2008, Reno, Nevada

AIAA 2008-1186

Exact Solutions for External Collisionless Gas Flows

Chunpei Cai * and Danny D. Liu†
ZONA Technology Inc., Scottsdale, Arizona, 85258
Iain D. Boyd‡
University of Michigan, Ann Arbor, Michigan, 48109

This paper concentrates on two external collisionless gas flow problems. The first problem concerns collisionless gas flows expanding into vacuum, which have important applications such as free molecular cold gas jet formed from electric propulsion devices; the second one considers collisionless flows over a flat plate. From a relation between particle position and velocity, we obtain the corresponding exact solutions for the number density and velocity distributions for both problems. Numerical simulation results obtained with the direct simulation Monte Carlo method validate the analytical solutions. In general, the comparisons between the exact analytical solutions and the numerical results are virtually identical. The same procedure developed in this paper can be used to study many other external collisionless flows.

Nomenclature

C_D, C_f, C_L	drag, friction and lift coefficients
f	velocity distribution function
n	number density
r, θ	polar coordinate variables
R	radius for a circular or an annular exit, or universal gas constant
T	macroscopic temperature
u, v, w	microscopic molecular velocity
U, V, W	macroscopic average velocity
y, z	a point on exit
X, Y, Z	a point in front of the exit
α	angle between the X-axis and a segment from (0,0) to (X,0,Z), or plate inclination angle
β	$1/(2RT_0)$
Ω	specific domain in velocity space

*Computational Fluid Dynamics Specialist, 8489 E. Ironwood Square Dr., AIAA Senior Member.
†President. Professor Emeritus Arizona State University, AIAA Fellow.
‡Professor, Department of Aerospace Engineering, 1320 Beal Ave., AIAA Associate Fellow.

Copyright © 2008 by chunpei cai. Published by the American Institute of Aeronautics and Astronautics, Inc., with permission.

subscript

0	averaged property at exit, or free stream value
w	wall property

I. Introduction

This paper concentrates on two collisionless gas flow problems, the first problem concerns collisionless gas flows out of a circular or annular exit, and other considers collisionless flows over a flat plate. This section briefly review the previous work in the literature.

These problems are relatively simple rarefied gasdynamic problems with mathematical significance and real applications, and many researchers have studied both problems. High speed collisionless, or free molecular, gas flows passing through small circular or annular apertures are fundamental problems with many real applications such as neutral gas expansion out of Electric Propulsion (EP) devices. Usually the cold plume flow out of an EP device is modeled by assuming free molecular flows with a nonzero, uniform average exit velocity, U_0. Even when the average bulk velocity of gas near the orifice is zero, the average velocity at the orifice exit plane is not zero, it corresponds to an outflow with a half Maxwellian distribution. As pointed out by Woronowicz,[1] for high speed plume flows, even though the number density at the exit can be high, the relative velocity is very small, and intermolecular collisions happen very rarely. In the past, analytical studies of similar problems were concentrated on true effusion problems with a zero average exit speed. For example, Liepmann[2] reported the efflux of gases through circular apertures, which is an example of a transition from the gasdynamic to the gaskinetic regime; Narasimha[3] obtained the exact solutions of density, velocity and temperature distributions for a free molecular effusion flow, and the results for a nearly free molecular effusion flow, expanding into vacuum through a circular orifice; Brook[4] reported the density field of free molecular flow from an annulus, to study the gas leakage effect from a spacecraft hatch. Other researchers reported many approximate methods or numerical simulations to study rarefied flows through a slit, for example, Rotenberg,[5] Hasegawa,[6] Cercignani[7] and Sharipov.[8] Recently, Lilly *et al* reported their work on measurement and computation of mass flow and momentum flux through short tubes in rarefied gas.[9] For the case of free molecular flows with a nonzero average velocity, usually the problems are very complicated, and approximations are often exercised such as neglecting the details of the exit geometry or assuming that free molecular flow is emitted from a point source.[10] The other problem, high speed collisionless external flow over a flat plate is also very important for space engineering, especially the aerodynamic coefficients, such as C_D, C_L, C_f, and heat flux rate are important for spacecraft design. For collisionless flows over a plate, the earliest work may date back to Kogan;[11] several more recent books discussed collisionless aerodynamics over a flat plate as well, such as those by Bird,[12] Gombosi[13] and Shen.[14] Especially, Bird[12] discussed plate surface properties for collisionless flows with both diffuse and specular reflections, and the direct simulation Monte Carlo (DSMC) method is probably the most appropriate numerical tool to simulate rarefied gas flows. Chen[15] disccused the surface drag and heat transfer for collisionless flows over a plate, cylinder and small sphere. It is also worthy to mention that Sun & Boyd[16] reported a study of rarefied gas flows over a 5% thickness flat plate with a hybrid method. However, in the literature, almost all the collisionless flows over a flat plate were focused on the wall properties.

In our previous study,[17,18]we adopted a relation between velocity-directions and geometry-locations to investigate free molecular plume flow problems. This treatment is more general than the solid angle treatment,[3] which was widely used in studying true collisionless effusion flows with a zero average exit speed, but is not applicable to collisionless flows with a nonzero average exit speed. In this study, we further investigate collisionless flows out of a circular or an annular exit with a nonzero average speed; and we also discuss the flows over a flat plate, especially for locations off the plate surface.

This paper is organized as follows: Section II describes the first problem, the corresponding exact solutions, approximate farfield solutions, and compares the analytical results with particle simulation results;

Section III discusses the second problem by applying the same principles, and presents some validations by again comparing the analytical results with particles simulation results; and Section IV summarizes this study.

II. Problem 1: Plume Flow Problems and Solutions

A. Free Molecular Problems

The first problem involves the following free molecular gas flows expanding into vacuum from an exit:

(1) A circular exit with a radius of R, average exit velocity U_0 that is greater than zero.

(2) An annular exit characterized by an inner radius R_1 and an outer radius R_2, average exit velocity U_0 that is greater than zero.

These two cases are closely related: if R_1 in the second case is set to zero, then it degenerates to the first case. Because both cases have important applications, we discuss both and provide the complete solutions.

The thermal velocity at the exits are expressed with a Maxwellian distribution function characterized by a number density n_0 and a temperature T_0:

$$f(u,v,w)dudvdw = n_0\left(\frac{\beta}{\pi}\right)^{3/2}\exp(-\beta(u^2+v^2+w^2))dudvdw \tag{1}$$

where $\beta = \frac{1}{2RT_0}$. Although the plume itself is in a highly non-equilibrium state, it is reasonable to assume the flow is at equilibrium before it escapes from the exit. Using T_0 and n_0 to describe this equilibrium state is a natural selection widely used by many researchers in the past.[13]

For this problem, we adopt the following coordinate systems: Denote the plume direction as the X-axis direction, the direction normal to the X-axis as the Z-axis direction, and the circle center/annulus center is the origin. The objective is to obtain the analytical plume field flow solutions, especially the number density and velocities at any point downstream of the exits.

B. Collisionless Effusion Flow Solutions

Narasimha adopted solid angles to study a free molecular flow of gas escaping from an orifice,[3] however, this solid angle approach is not general enough to study effusion flows with nonzero average exit velocities. Instead, a geometric relation between velocity and position was recently proposed.[17]

For the circular exit case with a nonzero average exit speed, the relation between velocity and position takes a new format. Suppose the average velocity at the circular exit is U_0, from any point $(0,y,z)$ on the circular exit which is characterized by a radius of R, only particles with the following special velocity components can arrive at a point $(X,0,Z)$ in front of the exit:

$$\frac{X}{u+U_0} = \frac{Y-y}{v} = \frac{Z-z}{w} \tag{2}$$

where $X>0, Y=0, Z>0$. Combined with the geometry relations:

$$z = r\sin\theta = Z - Xw/(u+U_0), y = r\cos\theta = Y - Xv/(u+U_0) \tag{3}$$

where $r\in[0,R]$, $\theta\in[0,2\pi]$, the integrals for the number density and the velocities can be simplified using the following change of variables:

$$dvdw = \begin{vmatrix} \frac{\partial v}{\partial r} & \frac{\partial v}{\partial \theta} \\ \frac{\partial w}{\partial r} & \frac{\partial w}{\partial \theta} \end{vmatrix} drd\theta = \frac{(u+U_0)^2}{X^2} rdrd\theta \tag{4}$$

The above change of integral variables transfers the integral domains from $(-\infty,+\infty)$ for v,w to finite spans for r and θ.

The final results of number density and velocities at a point $(X, 0, Z)$ in front of the exit are:

$$\begin{aligned} n(X,0,Z) &= \int_{-U_0}^{+\infty} du \int_{-\infty}^{+\infty} dv \int_{-\infty}^{+\infty} dw \left(\frac{\beta}{\pi}\right)^{3/2} \exp[-\beta(u^2+v^2+w^2)] \\ &= 2\left(\frac{\beta}{\pi}\right)^{3/2} \int_0^{\infty} dt \frac{t^2}{X^2} \int_{-\pi/2}^{\pi/2} d\theta \int_0^R r dr \exp[-\beta(t-U_0)^2 - \beta\frac{t^2}{X^2}(r^2+Z^2-2rZ\sin\theta)] \\ &= \frac{1}{X^2}\left(\frac{\beta}{\pi}\right)^{3/2} \int_{-\pi/2}^{\pi/2} d\theta \int_0^R \exp\left(-\beta U_0^2 \frac{r^2+Z^2-2Zr\sin\theta}{X^2+r^2+Z^2-2Zr\sin\theta}\right) r K dr \end{aligned} \tag{5}$$

$$U(X,0,Z) = \frac{1}{n(X,0,Z)X^2}\left[\left(\frac{\beta}{\pi}\right)^{3/2} \int_{-\pi/2}^{\pi/2} d\theta \int_0^R \exp\left(-\beta U_0^2 \frac{r^2+Z^2-2Zr\sin\theta}{X^2+r^2+Z^2-2Zr\sin\theta}\right) M r dr\right] \tag{6}$$

$$W(X,0,Z) = \frac{1}{n(X,0,Z)X^2}\left[\left(\frac{\beta}{\pi}\right)^{3/2} \int_{-\pi/2}^{\pi/2} d\theta \int_0^R \frac{Z-r\sin\theta}{X} \exp\left(-\beta U_0^2 \frac{r^2+Z^2-2Zr\sin\theta}{X^2+r^2+Z^2-2Zr\sin\theta}\right) M r dr\right] \tag{7}$$

where $K = \frac{Q^2 U_0}{\beta}\exp(-\beta U_0^2 Q) + (\frac{Q}{2\beta} + Q^2U_0^2)\sqrt{\frac{\pi Q}{\beta}}[1+erf(\sqrt{\beta Q}U_0)]$, $Q = \frac{X^2}{X^2+Z^2+r^2-2Zr\sin\theta}$, $M = \frac{Q^3U_0^2}{\beta}\exp(-\beta Q U_0^2) + \frac{Q^2}{\beta^2}\exp(-\beta Q U_0^2) + (\frac{3Q^2U_0}{2\beta} + Q^3U_0^3)\sqrt{\frac{\pi Q}{\beta}}[1+erf(\sqrt{\beta Q}U_0)]$.

Similarly the results for the annular case are straightforward to obtain by replacing the integral range for the exit radius from $0 < r < R$ in Eqns.(5, 6, 7) by $R_1 < r < R_2$.

C. Farfield Approximations

Although the above exact relations are accurate and convenient to evaluate via a computer program since the integration over the infinite span of velocity space is complete, they are rather complex for practical usage. Hence approximate farfield simplifications are developed. Here we provide these for the annular exit case, and the circular exit case can be obtained by setting $R_1 = 0$ in the following formula. From the above relations, with the far field approximation: $R_1 < r < R_2 \ll \sqrt{Z^2+X^2}$, $Q = \frac{X^2}{X^2+Z^2} = \cos^2\alpha$ and:

$$\begin{aligned} n(X,0,Z) &= \frac{R_2^2-R_1^2}{X^2}\cos^3\alpha\left[1 - \frac{\beta U_0^2}{X^2+Z^2}\left(\frac{R_1^2+R_2^2}{2}+Z^2\right)\right] \\ &\left(\frac{U_0}{2}\cos\alpha\sqrt{\frac{\beta}{\pi}}\exp(-\beta U_0^2\cos^2\alpha) + \left(\frac{1}{4}+\frac{\beta\cos^2\alpha U_0^2}{2}\right)[1+erf(\sqrt{\beta}\cos\alpha U_0)]\right) \end{aligned} \tag{8}$$

$$\begin{aligned} U(X,0,Z) &= \frac{1}{n(X,0,Z)}\sqrt{\frac{\beta}{\pi}}\frac{R_2^2-R_1^2}{2X^2}\cos^4\alpha\left[1 - \frac{\beta U_0^2}{X^2+Z^2}\left(\frac{R_1^2+R_2^2}{2}+Z^2\right)\right] \\ &\left[\left(\cos^2\alpha U_0^2 + \frac{1}{\beta}\right)\exp(-\beta\cos^2\alpha U_0^2) + \left(\frac{3\cos\alpha U_0}{2} + \beta U_0^3\cos^3\alpha\right)\sqrt{\frac{\pi}{\beta}}[1+erf(\sqrt{\beta}\cos\alpha U_0)]\right] \end{aligned} \tag{9}$$

$$\begin{aligned} W(X,0,Z) &= \frac{1}{n(X,0,Z)}\sqrt{\frac{\beta}{\pi}}\frac{R_2^2-R_1^2}{2X^2}\cos^4\alpha\left[\frac{Z}{X} - \frac{\beta U_0^2 Z}{X(X^2+Z^2)}\left(\frac{R_2^2+R_1^2}{2}+Z^2\right) - \frac{(R_2^2+R_1^2)Z}{2X(X^2+Z^2)}\right] \\ &\left[\left(\cos^2\alpha U_0^2 + \frac{1}{\beta}\right)\exp(-\beta\cos^2\alpha U_0^2) + \left(\frac{3\cos\alpha U_0}{2} + \beta U_0^3\cos^3\alpha\right)\sqrt{\frac{\pi}{\beta}}[1+erf(\sqrt{\beta}\cos\alpha U_0)]\right] \end{aligned} \tag{10}$$

The cosine function dominates in the farfield simplifications, and by retaining the geometry radius in the expressions, these relations are more accurate than the results obtained by Narashima.[10] By comparison, the point source solutions[10] totally neglect the exit geometry, hence their accuracy should be inferior to the above approximations.

D. Centerline Property Distributions

The centerline property distributions can be obtained from the exact solutions by setting $Z = 0$. The final exact solution to the circular exit case is:

$$n(X,0,0) = \frac{1}{2} + \frac{1}{2}erf(\sqrt{\beta}U_0) - \frac{X}{2\sqrt{X^2+R^2}}\exp(-\frac{\beta R^2 U_0^2}{X^2+R^2})[1+erf(\sqrt{\beta\frac{X^2}{X^2+R^2}}U_0)] \tag{11}$$

$$U(X,0,0)=\frac{1}{2n(X,0,0)}\left[\frac{R^2\exp(-\beta U_0^2)}{\sqrt{\beta\pi}(X^2+R^2)}+U_0[1+erf(\sqrt{\beta}U_0)]-\exp(-\frac{\beta R^2U_0^2}{X^2+R^2})\frac{U_0X^3}{(X^2+R^2)^{3/2}}\left[1+erf(\sqrt{\beta\frac{X^2}{X^2+R^2}}U_0)\right]\right] \tag{12}$$

The corresponding solutions for the annular exit case are:

$$\begin{aligned} n(X,0,0) &= \frac{X}{2\sqrt{X^2+R_1^2}}\exp(-\frac{\beta R_1^2U_0^2}{X^2+R_1^2})\left[1+erf(\sqrt{\beta\frac{X^2}{X^2+R_1^2}}U_0)\right] \\ &\quad -\frac{X}{2\sqrt{X^2+R_2^2}}\exp(-\frac{\beta R_2^2U_0^2}{X^2+R_2^2})\left[1+erf(\sqrt{\beta\frac{X^2}{X^2+R_2^2}}U_0)\right] \end{aligned} \tag{13}$$

$$\begin{aligned} U(X,0,0) &= \frac{1}{2n(X,0,0)}\left[\frac{X^2}{\sqrt{\beta\pi}}(\frac{1}{X^2+R_1^2}-\frac{1}{X^2+R_2^2})\exp(-\beta U_0^2)+\exp(-\frac{\beta R_1^2U_0^2}{X^2+R_1^2})\frac{U_0X^3}{(X^2+R_1^2)^{3/2}}\left[1+erf(\sqrt{\beta\frac{X^2}{X^2+R_1^2}}U_0)\right]\right. \\ &\quad \left.-\exp(-\frac{\beta R_2^2U_0^2}{X^2+R_2^2})\frac{U_0X^3}{(X^2+R_2^2)^{3/2}}\left[1+erf(\sqrt{\beta\frac{X^2}{X^2+R_2^2}}U_0)\right]\right] \end{aligned} \tag{14}$$

If $U_0=0$, the centerline results degenerate to those for effusion flow problems.[18]

E. Validation

Although the complete analytical results involve several integral terms that cannot be explicitly removed, numerical evaluations are convenient via a computer program. The subroutine for the error function can be found in many numerical computing books.[19] Because the flows are rarefied, it is appropriate to utilize the DSMC method[12] to validate the analytical results. In this study, we used a specific DSMC package named MONACO[20] to perform the simulations. The simulation domain and mesh are quite simple, and the collision function in MONACO is turned off to achieve the collisionless effect. Under this situation, the value of the number density at the exit does not produce any difference in the final normalized results and exact free molecular flows are guaranteed.

Figure 1 shows comparisons of number density contours from the exact analytical solutions, shown with solid lines on the top; the farfield approximation results, shown with dashed lines on the top; the point source solutions,[1] shown with dashed lines at the bottom; and the DSMC results, shown with solid lines at the bottom. The average exit velocity at the slit is set to $\sqrt{2RT_0}$ and the exit temperature is set to $T_0=300$ K. Generally the exact analytical results are almost identical to the DSMC simulation results. There are some minor differences at the near field close to the exit, because the numerical evaluation of the exact solutions contains very small denominator terms in these regions, especially close to the origin. It is also very clear from the plot that the farfield approximation is not very accurate when $X<3R$, but the accuracy significantly improves when $X>3R$. Another factor for the difference is that the farfield approximation is the result by reserving the first expansion term from the integration kernel, the exponent function; more terms can be included to achieve higher accuracy.The point source density contours have large discrepancies at the origin, because the denominator contains a factor of r, hence, for the point source expression, the density at the origin point approaches to infinity. However, for farfield locations, the point source solution performs very well, and it has a more concise format than the exact analytical solutions and the farfield approximations.[1]

Figures 2 and 3 show the corresponding results of velocity contours normalized with the characterized thermal speed $\sqrt{2RT_0}$. Similar conclusions to the density distributions can be drawn from these two pictures. The flow patterns have a narrow zone where exit effects dominate, but in the farfield, the contour lines are straight.

We also perform a simulation to validate the analytical results for the annulus case as well. In this simulation, the inner and outer radii of the annulus are set to $R_1=0.1$ m and $R_2=0.2$ m, respectively.

Figure 4 shows contours of normalized number density. In the whole simulation domain, the comparison shows very close results between the exact analytical solutions and the numerical simulations, and the farfield simplifications become very accurate when $X>3R_2$. Figures 5 and 6 show the velocity contours. Both

comparisons are very satisfactory as well. In all of these three pictures, both the exit region and the slow "cavity" region in the center, which is characterized by negative W_z, are clearly captured.

III. Flow Over a Flat Plate

A. Problem and Solutions

The second problem is illustrated by Fig.7: A zero-thickness flat plate AB is set with an inclination angle $\angle BOF = \alpha$, the plate length is L, and we set the coordinate center at the plate center. Collisionless gas, assumed to be argon in this study, flows from the left to the right, with a macroscopic average velocity U_0, a temperature of T_0 and a number density of n_0. To aid the study, we assume the outer boundary as a circle with a very large radius. At each point on the circle, incoming particles follow a Maxwellian distribution function characterized by the free stream parameters, T_0, U_0 and n_0. Suppose an arbitrary point $P(x, y)$ is off the plate, either in the front or the back side of the plate. In this study, we assume the reflections at the flat plate are completely diffuse.

By following the same principles used in the first problem, we can solve this problem as well. From Fig.7, on the large circle, at a point (X, Y), of all particles with a thermal velocity (u, v), only those satisfying the following relation can reach point $P(x, y)$, if (X, Y) is visible from $P(x, y)$:

$$(u + U_0)/(X - x) = v/(Y - y) \tag{15}$$

If a particle's velocity components satisfy the above relation, then it cannot miss passing through $P(x, y)$ neither, unless it is not on the same side of the plate as point $P(x, y)$. Since all incoming particles on the large circle follow the free stream Maxwellian distribution function, then with the above relation, the effects of free stream can be described by the velocity space shown on the left side of Fig.8, within a domain Ω_1. With a similar relation,

$$u/(X - x) = v/(Y - y) \tag{16}$$

the contributions to point $P(x, y)$ by those diffusely reflected particles from the plate are described by an Maxwellian distribution function with a domain, Ω_2, shown on the right side of Fig.8. The boundaries of these two domains, Ω_1 and Ω_2, are determined by point $P(x, y)$, the two specific plate ends $A(Ax, Ay)$ and $B(Bx, By)$, and the above two equations. If we denote $\theta_1 = atan^{-1}[(y - Ay)/(x - Ax)]$ and $\theta_2 = atan^{-1}[(y - By)/(x - Bx)]$, where $atan^{-1}$ is a function with a value range of $[-\pi, \pi]$, then from the two equations, $\angle NPO = \angle LOu = \theta_1$ and $\angle MPO = \angle KOu = \theta_2$. From Eqn.15, we can conclude, point $(-U, 0)$ belongs to domain Ω_1. Hence, the boundaries for Ω_1 and Ω_2 are completely determined by Eqns.(15) and (16). When $U_0 = 0$, then Ω_1 and Ω_2 do not overlap, a combination of these two domains leads to a complete domain where u, v both have a range of $(-\infty, +\infty)$.

The velocity distribution function for point $P(x, y)$ consists of contributions from two different Maxwellian distribution functions:

$$f_0(u, v) = n_0(\beta_0/\pi)^{3/2} \exp[-\beta_0(u^2 + v^2 + w^2)], (u, v) \in \Omega_1 \tag{17}$$

$$f_w(u, v) = n_w(\beta_w/\pi)^{3/2} \exp[-\beta_w(u^2 + v^2 + w^2)], (u, v) \in \Omega_2 \tag{18}$$

where $\beta_0 = 1/(2RT_0)$, $\beta_w = 1/(2RT_w)$, and

$$n_w = n_0\sqrt{T_0/T_w}[\exp(-S^2S_\alpha) \pm \sqrt{\pi}(SS_\alpha)(1 + erf(\pm SS_\alpha))], \tag{19}$$

the "+" sign is used for the front side and "-" for the back side, $S = U_0/\sqrt{2RT_0}$ is the speed ratio, and $S_\alpha = S\sin(\alpha)$. See the books by Kogan[11] or Bird[12] for details.

Integrating the above two velocity distribution functions, Eqns.(17) and (18), over $1, u, v$, leads to the macroscopic number density, U-velocity and V-velocity distribution functions:

$$\begin{aligned} n(X, Y) &= \int_{\Omega_1} f_0 du dv + \int_{\Omega_2} f_w du dv \\ &= n_0 - n_0 \exp(-\beta_0 {U_0}^2)[(\theta_2 - \theta_1) + \sqrt{\pi/\beta_0}\gamma(\theta_1, \theta_2)]/(2\pi) + n_w(\theta_2 - \theta_1)/(2\pi) \end{aligned} \tag{20}$$

where $\gamma(\theta_1,\theta_2)=\int_{\theta_1}^{\theta_2}\exp(\beta_0{U_0}^2\cos^2\theta)\beta_0U_0\cos\theta[1+erf(\sqrt{\beta_0}U_0\cos\theta)]d\theta$.

$$\begin{aligned}\frac{U(X,Y)}{\sqrt{2RT_0}} &= \frac{1}{n\sqrt{2RT_0}}\left(\int_{\Omega_1}uf_0dudv+\int_{\Omega_2}uf_wdudv\right)\\ &= \frac{n_0U_0}{n\sqrt{2RT_0}}-\frac{\exp(-\beta{U_0}^2)}{2n\pi\sqrt{2RT_0}}\left[\sqrt{\beta\pi}\int_{\theta_1}^{\theta_2}\left(U_0^2\cos^3\theta(1+erf(\sqrt{\beta}U_0\cos\theta))\exp(\beta{U_0}^2\cos^2\theta)\right)d\theta\right.\\ &\left.+\gamma(\theta_1,\theta_2)\frac{\sqrt{\pi/\beta}}{2\beta U_0}+\frac{U_0(\theta_2-\theta_1)}{2}+\frac{U_0(\sin(2\theta_2)-\sin(2\theta_1))}{4}\right]+\frac{n_w(\sin\theta_2-\sin\theta_1)}{4\sqrt{\pi}n}\end{aligned}\tag{21}$$

$$\begin{aligned}\frac{V(X,Y)}{\sqrt{2RT_0}} &= \frac{1}{n\sqrt{2RT_0}}\left(\int_{\Omega_1}vf_0dudv+\int_{\Omega_2}vf_wdudv\right)\\ &= -\frac{n_0}{4\sqrt{\pi}n}\left[\exp(-\beta_0{U_0}^2\sin^2\theta_1)\cos\theta_1(1+erf(\sqrt{\beta}U_0\cos\theta_1))\right.\\ &\left.-\exp(-\beta_0{U_0}^2\sin^2\theta_2)\cos\theta_2(1+erf(\sqrt{\beta}U_0\cos\theta_2))\right]+\frac{n_w(\cos(\theta_1)-\cos(\theta_2))}{4\sqrt{\pi}n}\end{aligned}\tag{22}$$

Details of the integration processes can be found in our previous work for a similar problem.[18] The effects from the plate length, L, are implicitly contained in the parameters θ_1,θ_2. By comparison, the classical surface properties of collisionless flows over a flat plate do not contain any plate length effects. The average translational temperature result is very complex and is omitted here, but we will show the simulation result for the temperature in the next section.

When $U_0=0$, the above results are greatly simplified as:

$$n(x,y)=n_0+(n_w-n_0)(\theta_2-\theta_1)/(2\pi)\tag{23}$$

$$U(x,y)=V(x,y)=0\tag{24}$$

$$T(x,y)=T_0+(T_wn_w-T_0n_0)(\theta_2-\theta_1)/(2\pi n)\tag{25}$$

B. Validations

To validate the above analytical results, we perform four numerical simulations with the MONACO package. The incoming flow is supposed to be argon, with a static temperature, $T_0=200$ K, and the plate temperature is set to $T_w=300$ K. The simulation domain is 5 meters by 5 meters with a total number of 100×100 cells, mainly to provide a high resolution. About 5 millions particles are used in each of these simulations, and the four sides of the outer domain are set to inlet boundary conditions. The other parameters are:

Case 2A: $U_0=0$ m/s, plate length $L=1$ m, plate inclination angle $\alpha=30^0$.

Cases 2B, 2C, 2D: $U_0=\sqrt{2RT_0}=288.34$ m/s, plate length $L=2$ m, plate inclination angles are $\alpha=0^0$, 30^0 and 90^0 respectively.

In the simulations, the plate thickness is assumed to be zero, but in the following pictures, a thick line is added to each picture to clearly illustrate the plate location.

Figures 9, 10 and 11 show contours for the number density normalized by the free stream value, n_0, the averaged translational temperature, in Kelvin, and the pressure normalized by n_0mRT_0, for test case 2A. As we can see, with a zero velocity in the free stream, the flow patterns are very simple, and the match between the analytical and DSMC simulation results are very good with some minor discrepancies. The contours shown in these three figures are actually circular, because along a circular line, the same solid angle is formed by different points and the two plate ends. Correspondly, the velocity phase spaces contains the same portion of solid angles for the free stream and the plate. Hence, the density, pressure and temperature must be the same. For this case, the macroscopic velocity at any point in the flowfield is absolutely zero, hence, the DSMC method cannot provide accurate velocity results due to the large statistical scatters, i.e., it is impossible to reduce the statistical scatter in the sampled velocity results to a certain fraction of the physical macroscopic averaged velocity value, say 5%. This explains the minor discrepancies between the analytical and DSMC results for the temperature and pressure: in the DSMC results, the inaccurate velocity values contribute

some effects to the temperature and pressure results, and they destroy the perfect symmetric patterns shown in the analytical results. In fact, this test case is more expensive than the other three test cases. The current Information Preservation (IP) method[21,22,23,24] has problems to simulate this case as well, because currently a specific step to accelerate particles' preserved velocities according to preserved pressure is needed for the IP method. As a result, the IP method may produce nonzero velocity results similar to the DSMC method. This test case 2A provides a very good benchmark case to further develop the IP method as well.

Figures 12, 13, 14 and 15 show the results of normalized number density, and velocity components, and temperature for test case 2B. Macroscopic properties of higher order moments of the distribution functions, such as pressure and temperatures, are neglected here for simplicity, even though in principal they are computable with more complex relations. The flow patterns for this test case are very complex indeed: a source at the front tip and a sink at the rear tip are visible, the nonzero free stream pushes the contour lines backward, and because the plate inclination angle is zero, the flow patterns are exactly symmetric about the X-axis. These contours show excellent matches between the analytical and numerical results, and we can confidently conclude that they accurately represent physical results. It is very evident that the contours have very complex patterns; by comparison, the results for the front and back sides of the plate have two specific point values, which are special cases of the general results from this study. For example, the front surface properties are the special values obtained by $\theta_1 = \alpha$ and $\theta_2 = \alpha + \pi$. It is rather surprising that such a simple collisionless flow can possess such complex flow patterns. The analytical solutions consist of factors from geometry relations, the free stream number density, n_0, mean velocity, U_0, temperature, T_0, and the plate temperature, T_w. The anlytical result for temperature is difficult to obtain due to more complex integrations, and here Fig. 15 only shows the simulation results. However, since temperature is a result of integrations of the velocity distribution functions with a higher order moment, we can believe that the future final analytical results should match the DSMC simulation results as well.

Figures 16, 17, 18 and 19 show the results of normalized number density, and velocity components, and temperature for test case 2C. With a plate inclination angle of 30^0, the symmetric patterns disappear as expected. The plate facing the incoming flow has a higher density, and the leeward side has a lower number density; the front side has smaller values of U-velocity due to the blocking effects by the plate, while the back side has larger values of U-velocity as the gas experiences expansion. The temperature contours include DSMC simulation results only and there are complex patterns as well. In general, the matches between analytical and numerical results are almost identical.

Figures 20, 21, 22 and 23 show the results of normalized number density, velocity components, and temperature for the last test case, which has a plate inclination angle of 90^0. The density contours have only two lines of value 1.0, while there are four for Cases 2B and 2C. The V-velocity contours have four specific lines of zero-values, which are very evident in Cases 2B and 2C as well. Again, we can conclude that both the analytical results and the simulation results are correct because the matches are excellent.

IV. Summary

The study for the first problem is a natural extension of the previous work[17] aiming to seek analytical results for free molecular plume flows from EP devices designed for spacecraft propulsion. We have reported analytical solutions to two fundamental free molecular flows out of a circular or an annular exit with nonzero average speed and validations with particle simulations. More specifically,

1). The analytical results indicate that the solutions are composed of complex geometry factors and the average exit velocity U_0. Even though the formulae are complex, we evaluated the analytical results and compared them with the DSMC simulation results. The excellent match between the numerical results and the analytical results indicates that the treatment in this study was correct. The accuracy of the exact solutions provides a solid foundation for farfield approximations and centerline property distributions.

2). The far field solutions of number density and velocities contain the exit geometry factors. Hence they are more accurate than the point source solutions obtained by Narasimha.[10] Comparisons with numerical simulation results indicate that the farfield approximations are accurate when $X > 3R$ for a circular exit

and $X > 3R_2$ for an annular exit.

We have reported a study of collisionless flows over a flat plate at different inclination angles as well, by applying the same principles used for the first problem. The collisionless flows over a plate have very complex density, velocity and temperature patterns, and the almost identical matches between the analytical and DSMC simulation results indicate the approach we used in this study is correct.

The approach used in this study is general and very heuristic, and can be used to study other collisionless external flows over objects of different geometries. Further, these results can be used as base solutions to solve for less rarefied flow situations, for example, with a linearized Boltzmann equation method.

Acknowledgment

This work is supported by the Internal Research and Development funding from ZONA Technology Inc.

References

[1]Woronowicz, M. S., "On Plume Flowfield Analysis and Simulation Techniques," AIAA paper 1994-2048, 6th AIAA/ASME Joint Thermophysics and Heat Transfer Conference, June 20-23, 1994, Colorado Springs, CO.

[2]Liepmann, H. W., "Gas kinetics and Gasdynamics of Orifice Flow," *J. Fluid Mech.*, Vol. 10, pp.65–79, 1961.

[3]Narasimha, R., "Orifice Flow of High Knudsen Number," *J. Fluid Mech.* Vol.10, pp.371–384, 1961.

[4]Brook, J. W., "Density Field of Directed Free-Molecular Flow from an Annulus," *Journal of Spacecraft*, Vol. 6, No. 6, pp.755-757, 1969.

[5]Rotenberg, A. N and Weitzner, H., "Nearly Free Flow Through an Orifice," *Physics of Fluids*, Vol. 12, 1573–1581, 1969.

[6]Hasegawa, M. and Sone, Y., "Rarefied Gas Flow Througth a Slit," *Physics of Fluids A*, 3(3), March 1991, pp.466-477.

[7]Cercignani, C. and Sharipov, F., "Gaseous Mixture Slit Flow at Intermediate Knudsen Numbers," *Physics of Fluids A*, 4 (6), June 1992, pp. 1283-1289.

[8]Sharipov, F., "Non-isothermal Rarefied Gas Flow Throught a Slit," *Physics of Fluids*, 9 (6), June, 1997, pp. 1804-1810.

[9]Lilly, T.C., Gimelshein, S.F., Ketsdever, A.D. and Markelov, G.N., "Measureemtns and Computations of Mass Flow and Momentum Flux Througth Short Tubes in Rarefied Gases," *Physics of Fluids*, 18 (9) 093601, 2006.

[10]Narasimha, R., "Collisionless Expansion of Gases into Vacuum," *J. Fluid Mech.* Vol. 12, pp.294–308, 1962.

[11]Kogan, M. N., *Rarefied Gas Dynamics*, Plenum press, New York, 1969.

[12]Bird, G. A., *Molecular Gas Dynamics and the Direct Simulation of Gas Flows,* Oxford University Press, New York, 1994.

[13]Gombosi, T. I., *Gaskinetic Theory,* Cambridge University Press, New York, 1994.

[14]Shen, C., *Rarefied Gas Dynamics-Fundamentals, Simulations and Micro Flows*, Springer, 2005.

[15]Chen, X., *Gaskinetics and Its Applications in Heat Transfer and Flows*, Tsinghua University, 1996.

[16]Sun, Q. and Boyd, I.D, "Flat-plate aerodynamics at very low Reynolds number," *J. Fluid Mech.*, Vol. 502, 199–206, 2004.

[17]Cai, C. and Boyd, I. D.,"Theoretical and numerical study of free-molecular problems," *J. Spacecraft Rockets*, Vol.44, No.2, 619-624, 2007.

[18]Cai, C., Theoretical and Numerical Studies of Plume Flows in Vacuum Chambers. Ph.D. Dissertation, Dept. of Aerospace Engineering, University of Michigan, Ann Arbor, Michigan, October, 2005.

[19]Press, W. H., Vetterling, S. A., Flannery, W. T. and Flannery, B. P., *Numerical Recipes in C,* Cambridge University Press, New York, 1994.

[20]Dietrich, S. and Boyd, I. D., "Scalar and Parallel Optimized Implementation of the Direct Simulation Monte Carlo Method," *J. Comput. Physics*, Vol.126, pp.328–342, 1996.

[21]Fan, J. and Shen, C., "Statistical simulation of low-speed unidirectional flows in transitional regime," 21st International Sympo. on Rarefied Gas Dynamics, pp245–252, 1998.

[22]Cai, C., Boyd, I. D, Fan, J. and Candler, G. V., "Direct simulation methods for low-speed microchannel flows," *J. Thermophy. Heat Tranfser*, Vol.14, pp.368-378, 2001.

[23]Fan, J. and Shen, C., "Statistical simulation of low-speed rarefied gas flows," Vol. 167, pp.393-399, 2002.

[24]Sun, Q. and Boyd, I. D., "A direct simulation method for subsonic, microscale gas flows," *J. Compt. Phys.*, Vol. 179, pp.400-425, 2004.

[25]Cai, C. and Boyd, I. D., "Collionless gas expanding into vacuum," *J. Spacecraft Rockets*, Vol.44, No.6, November-December, pp 1326-1330.

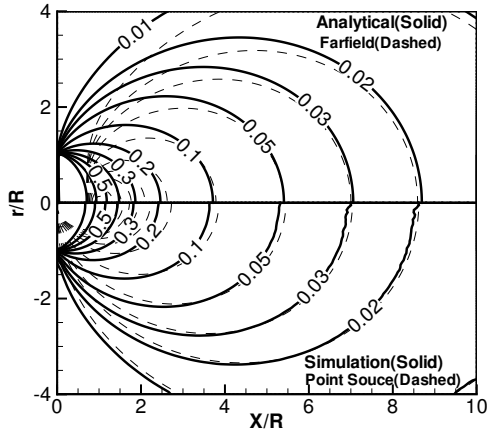

Figure 1. Contours of $n(X,0,Z)/n_0$ (Circular Exit, $U_0 = \sqrt{2RT_0}$).

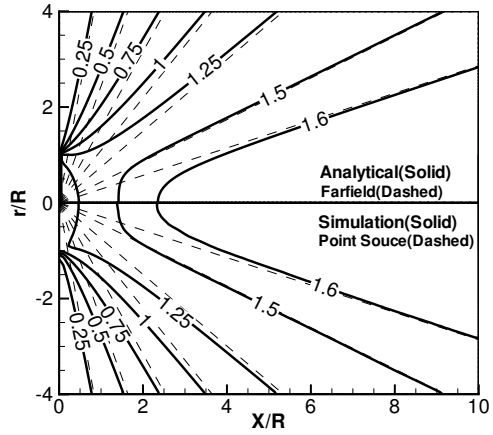

Figure 2. Contours of $U(X,0,Z)/\sqrt{2RT_0}$ (Circular Exit, $U_0 = \sqrt{2RT_0}$).

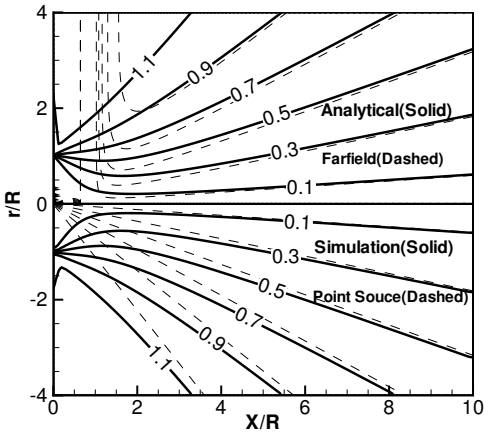

Figure 3. Contours of $W(X,0,Z)/\sqrt{2RT_0}$ (Circular Exit, $U_0 = \sqrt{2RT_0}$).

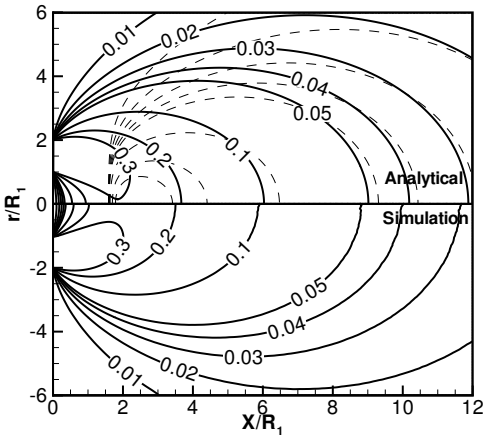

Figure 4. Contours of $n(X,0,Z)/n_0$ (Annular Exit, $R_2 = 2R_1$, $U_0 = \sqrt{2RT_0}$, Dashed Line: Analytical Farfield Approximations).

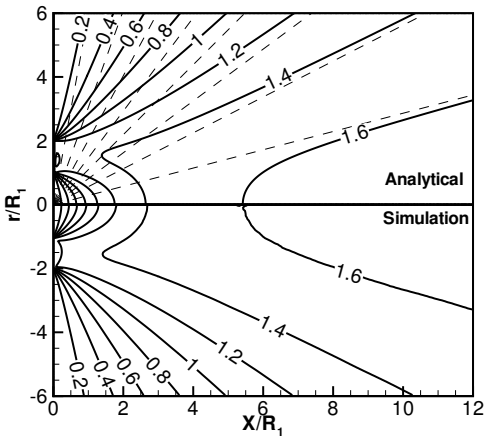

Figure 5. Contours of $U(X,0,Z)/\sqrt{2RT_0}$ (Annular Exit, $R_2 = 2R_1$, $U_0 = \sqrt{2RT_0}$, Dashed Line: Analytical Farfield Approximations).

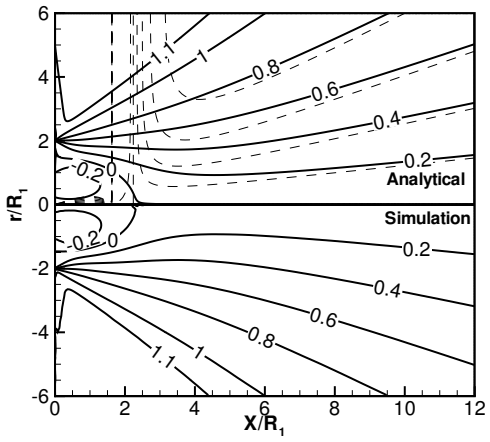

Figure 6. Contours of $W(X,0,Z)/\sqrt{2RT_0}$ (Annular Exit, $R_2 = 2R_1$, $U_0 = \sqrt{2RT_0}$, Dashed Line: Analytical Farfield Approximations).

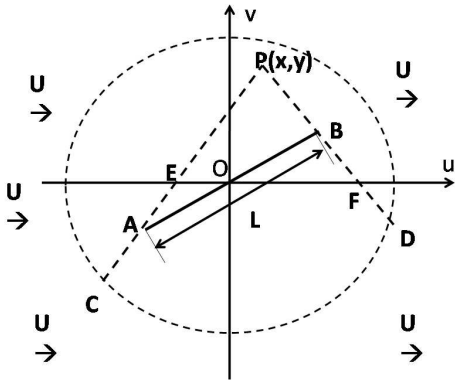

Figure 7. Illustration for the Second Problem.

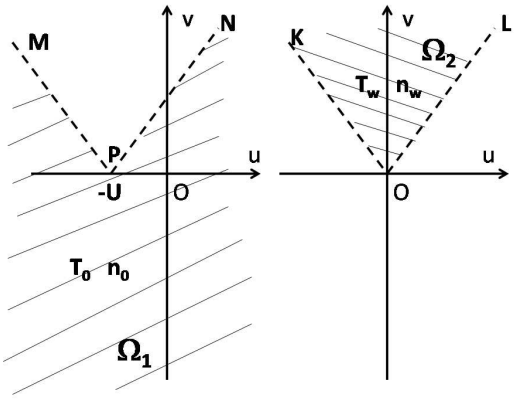

Figure 8. Typical Velocity Phase Space for the Second Problem.

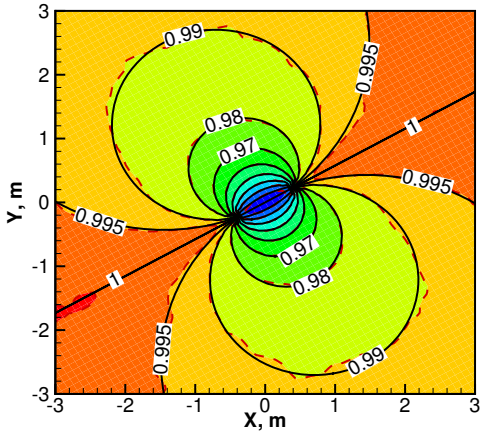

Figure 9. Case 2A: Normalized Density. Solid Line: Analytical, Dashed Line and Flood: DSMC.

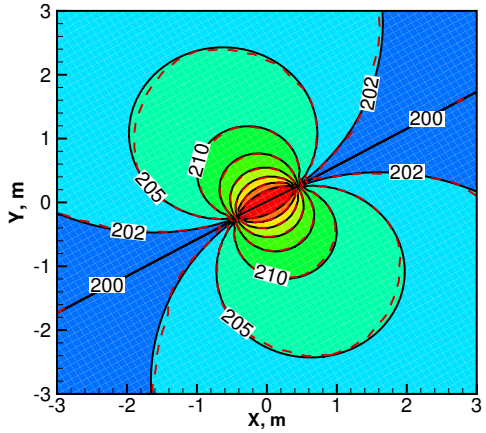

Figure 10. Simulation Results of Temperature, in Kelvin, for Case 2A.

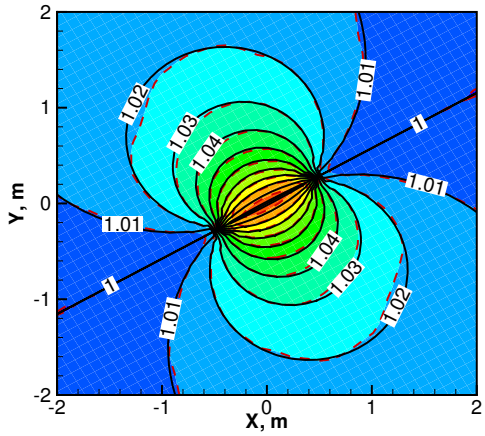

Figure 11. Contours of Normalized Pressure for Test Case 2A. Solid Line: Analytical, Dashed Line and Flood: DSMC.

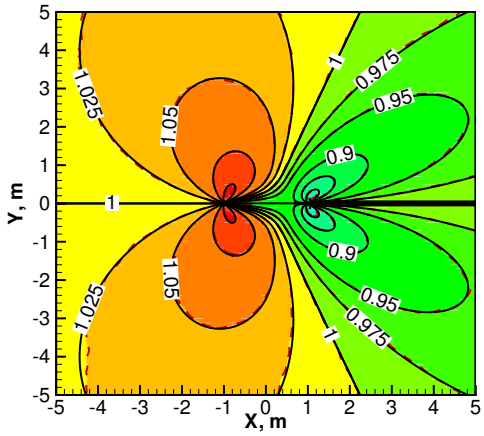

Figure 12. Contours of Normalized Number Density for Test Case 2B, Solid Line: Analytical, Dashed Line and Flood: DSMC.

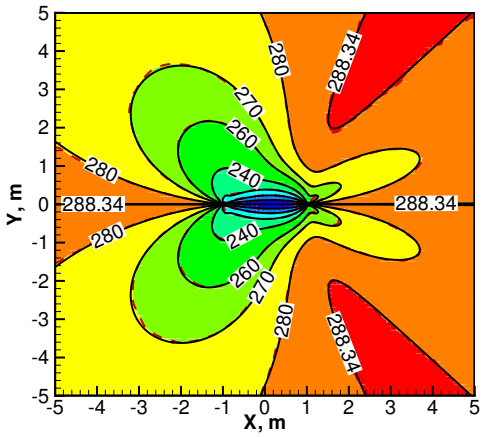

Figure 13. Contours of U-velocity, in m/s, for Test Case 2B, Solid Line: Analytical, Dashed Line and Flood: DSMC.

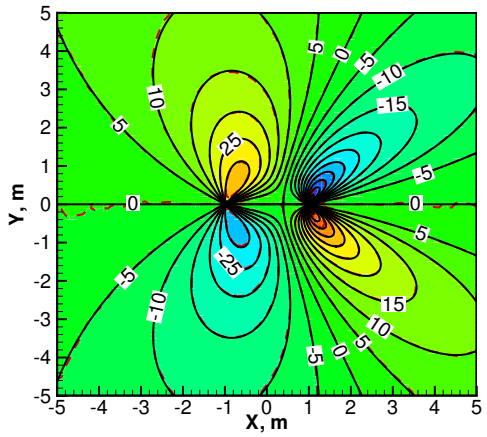

Figure 14. Contours of V-velocity, in m/s, for Test Case 2B, Solid Line: Analytical, Dashed Line and Flood: DSMC.

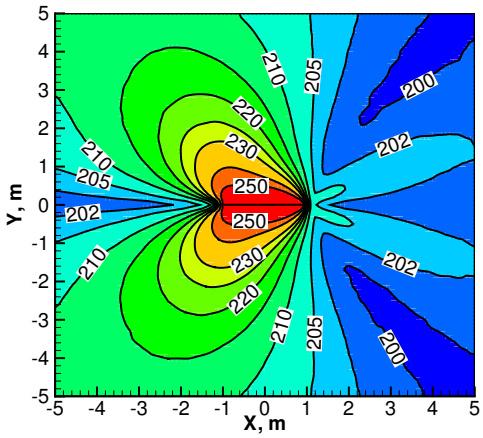

Figure 15. Simulation Results of Temperature, Kelvin, for Test Case 2B.

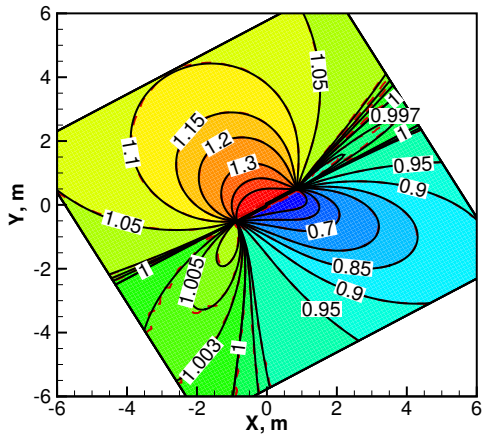

Figure 16. Contours of normalized number density, for Test Case 2C, Solid Line: Analytical, Dashed Line and Flood: DSMC.

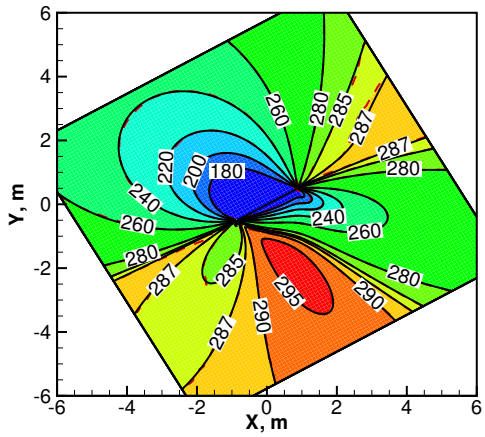

Figure 17. Contours of U-velocity, in m/s, for Test Case 2C, Solid Line: Analytical, Dashed Line and Flood: DSMC.

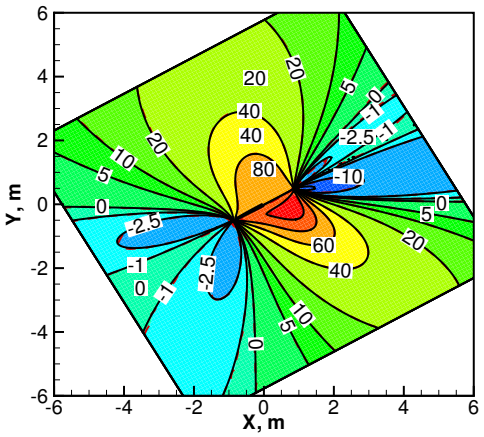

Figure 18. Contours of V-velocity, in m/s, for Test Case 2C, Solid Line: Analytical, Dashed Line and Flood: DSMC.

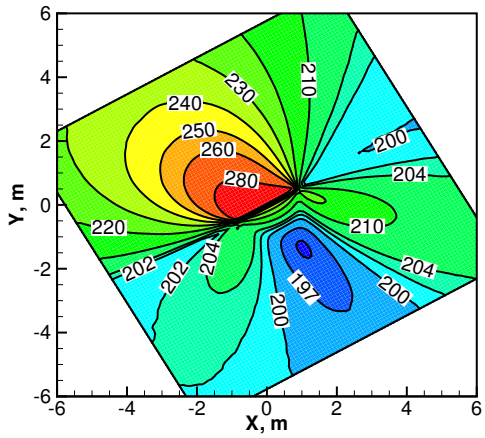

Figure 19. Simulation Results of Temperature, in Kelvin, for Test Case 2C.

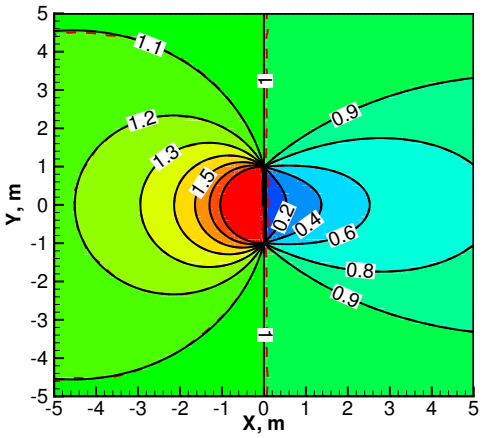

Figure 20. Contours of normalized number density for Test Case 2D, Solid Line: Analytical, Dashed Line and Flood: DSMC.

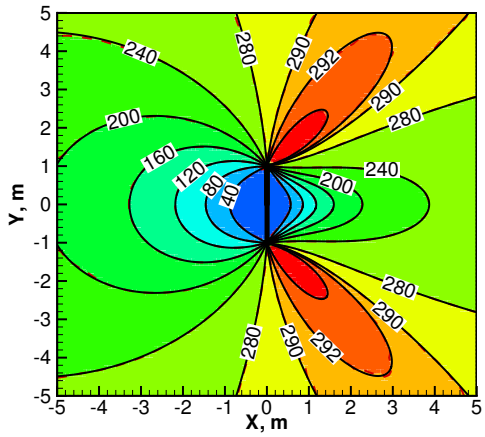

Figure 21. Contours of U-velocity, in m/s, for Test Case 2D, Solid Line: Analytical, Dashed Line and Flood: DSMC.

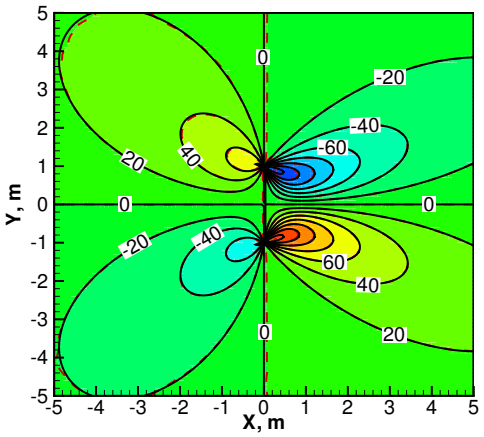

Figure 22. Contours of V-velocity, in m/s, for Test Case 2D, Solid Line: Analytical, Dashed Line and Flood: DSMC.

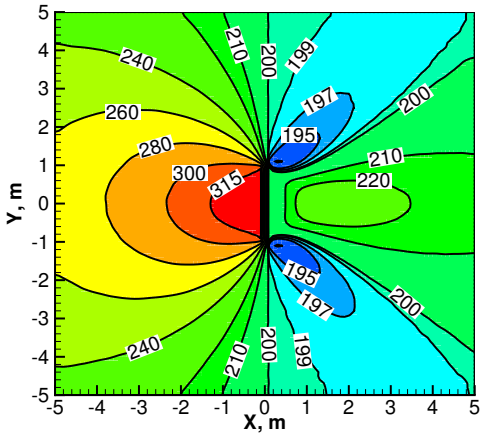

Figure 23. Simulation Results of Temperature, in Kelvin, for Test Case 2D.